2021-24-0089 Published 05 Sep 2021

Numerical Assessment of an After-Treatment System Equipped with a Burner to Speed-Up the Light-Off during Engine Cold Start

Augusto Della Torre, Loris Barillari, Gianluca Montenegro, and Angelo Onorati Politecnico di Milano

Federico Rulli, Stefano Paltrinieri, Vincenzo Rossi, and Francesco Pulvirenti Ferrari S.p.A.

Citation: Della Torre, A., Barillari, L., Montenegro, G., Onorati, A. et al., "Numerical Assessment of an After-Treatment System Equipped with a Burner to Speed-Up the Light-Off during Engine Cold Start," SAE Technical Paper 2021-24-0089, 2021, doi:10.4271/2021-24-0089.

Abstract

In the next years, the upcoming emission legislations are expected to introduce further restrictions on the admittable level of pollutants from vehicles measured on homologation cycles and real drive tests. In this context, the strict control of pollutant emissions at the cold start will become a crucial point to comply with the new regulation standards. This will necessarily require the implementation of novel strategies to speed-up the light-off of the reactions occurring in the after-treatment system, since the cold start conditions are the most critical one for cumulative emissions. Among the different possible technological solutions, this paper focuses on the evaluation of the potential of a burner system, which is activated before the engine start. The hypothetical burner exploits the lean combustion of an air-gasoline mixture to generate a high temperature gas stream which is directed to the catalyst section promoting a fast heating of the substrate. In this work, an experimental test bench has been adopted to characterize the thermal transient of the after-treatment system when the burner-like system is activated, monitoring the temperature of the gas flow and the temperature of the metallic walls at different locations. Moreover, a CFD model has been developed to investigate the light-off of the reactions during the initial operation of the burner and the subsequent start of the engine. The model, developed on the basis of the OpenFOAM code, resorts to a multi-region approach, where different meshes are employed to describe the fluid domain and the solid regions, namely the catalytic porous substrates and the metallic walls constituting pipes and canning. Specific submodels are implemented to consider flow resistance, heat transfer, mass transfer and catalytic reactions occurring in the catalyst region. The CFD framework has been initially validated on the experimental data acquired on the test bench. The methodology has been then applied to the preliminary analysis of the catalyst light-off at engine cold start, considering a full exhaust line equipped with burner-like system.

Introduction

By the end of the decade, the current emission legislation for the automotive sector is expected to evolve worldwide towards a more restrictive scenario, with a further limitation of the admitted levels for pollutant and greenhouse emissions [1, 2]. In Europe, this revision process of the current regulation will lead to the definition of the novel Euro 7 legislation, expected to be introduced in 2025-2027. In this perspective, the after-treatment operation at engine cold start represents an important area for achieving a further reduction of the pollutant emissions measured on standard homologation cycles and real drive tests. With regards to gasoline spark-ignition engines (SI) the current after-treatment technology relies on the three-way catalyst (TWC), usually coupled with a particle filter (GPF) for the removal of particle matter (PM). TWC is effective at relatively high catalyst brick temperature (higher than 500-600 K) and, therefore, it does not guarantee a sufficient pollutant conversion at the cold start [3]. Thus, the increase of the catalyst efficiency at cold start requires the implementation of suitable technological solutions. In this context, different strategies have been explored in the literature to speed-up the light-off of the catalyst. The simplest strategy is represented by the adoption of in-cylinder thermal management solutions, based on a proper control of A/F ratio, spark advance and valve actuation in such a way to increase the exhaust temperature for some operating conditions [4]. This solution can be made more effective by a proper control of cylinder deactivation, exploiting the dynamic skip fire of the cylinders [5]. Another strategy, largely applied in the last years with the progressive hybridization of the power units, is represented by electrical heating catalyst solutions [6]. This technology has the significant advantage to be activated with a certain time advance with respect to the engine start, allowing to increase the conversion efficiency in the very early phase of the driving cycle. On the other hand, its usual structural shape made of metallic spiral coils can originate local hot spots which, even if beneficial for the catalyst light-off [7] may be problematic from the point of view of the mechanical stress. Another possible solution, which shares the advantages of electrical heating, is represented by burner heating. This

technology was at first proposed in the early nineties [8, 9] and then investigated in the following decade [10], showing a good potential in achieving high catalyst efficiency at the cold start. However, at that time, the implementation of simple in-cylinder thermal strategies was sufficient to accomplish the emission regulations and, therefore, there are not example of application of this solution on production vehicles. Nowadays, in light of the novel emission regulation, this strategy can be regarded with renewed interest, even if associated to significant technological challenges. In particular, the control of the burner and the stability of its operation is an issue which still requires specific developments and investments: this is confirmed by the fact that this solution is not proposed yet on the market by any components manufacturer (on the contrary of electrical heating solutions) and, also, there is not recent scientific literature on the topic.

With these premises, this work focuses on the operation of an after-treatment system equipped with a catalyst burner-like system with the aim to evaluate its potential for the speed-up of the catalyst light-off. In this preliminary study the device is investigated under lab conditions considering a specific test bench, where the operation of the burner can be suitably controlled in all the running phases. The investigation was carried out on the basis of a CFD numerical analysis supported by experimental activity for the validation of the models. The study is focused on the after-treatment system of a high-performance SI gasoline engine, in order to investigate the behavior of the system during the cold start phase. To this purpose, an advanced CFD model is developed on the basis of the open-source OpenFOAM code, with the aim of describing the complex multi-physics nature of the problem which involves different phenomena occurring at different scales, including: mass/heat transfer, chemical reactions, flow through porous media, etc. The numerical model allows the detailed description of the after-treatment geometry by means of a fully-3D approach, making it possible to describe the flow and temperature distribution in the system, enabling the optimization of the configuration. Moreover, it implements advanced catalyst models to evaluate the non-uniformity of the pollutant conversion occurring on the catalytic substrate. The solution algorithm is optimized in order to allow the simulation of quite long time interval, in the order of magnitude of minutes, in such a way to be applied to the analysis of significant portions of the homologation / real driving cycle.

The work is structured as follows. At first, methodology is presented, discussing all the significant details of the implementation of the numerical model and describing the experimental setup. Then, an overview of the case study is given, discussing the configurations considered for the different steps of the analysis, namely validation and application. Finally, the simulation campaign is reported, focusing on the details of the light-off process during the engine cold start and highlighting the effects of the burner pre-heating.

Methodology

The analysis of the after-treatment system equipped with burner heating was performed with a combination of CFD investigations and experimental characterization. In particular, experimental measurements were exploited for the model validation, with specific regards on the thermal aspects. Alongside, CFD analysis were applied for a comprehensive study of all the complex aspects involved (i.e. heat-/mass-transfer, chemical reactions, flow through porous media) and of their interaction, to provide a deep insight of the phenomena occurring at the engine cold start.

Simulation Model

The computational model adopted in this work is based on the open-source CFD code OpenFOAM [11] and it consists of an evolution of a previous model developed by the authors as reported in [7, 12]. In particular, the modeling approach resorts to a multi-region framework (Figure 1), in which multiple computational grids are adopted to describe the different physical domains, namely: a) the fluid, which describes the gas flow through the system; b) the solid, which describes the metallic walls constituting pipes and cannings; c) the substrate, which describes the catalyzed porous media (honeycomb or open-cell foam) on which surface reactions take place.

The computational meshes can be adjacent or overlapping: the former is typically the case of the solid metallic walls which bounds the fluid domain while the latter is necessary for describing porous substrates, where the fluid and solid phases coexist in the same zone. This multi-region framework allows to take into account the thermal inertia of the different solid components included in the after-treatment, being metal walls or substrates, making it possible to accurately describe the thermal transient of the system at the cold start of the engine and its effect on the light-off of the catalytic reactions.

Governing Equations The multi-region problem requires to solve different governing equations for the different domains and to define proper coupling models for describing their interactions. Figure 2 reports the structure of the computational model, highlighting the governing equations for domains of type fluid, substrate and solid along with the specific source terms adopted for the modeling of typical physical phenomena. In particular, referring to the fluid region, the computational model includes the conservation equations for the momentum, the energy and the chemical

FIGURE 1 Multi-region framework for after-treatment CFD modeling.

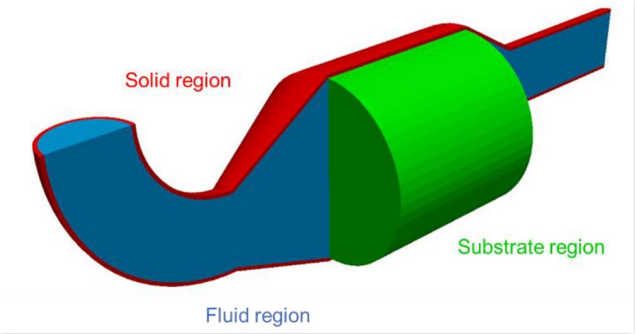

FIGURE 2 Overview of the governing equations solved for each domain and of the coupling terms for describing their interaction.

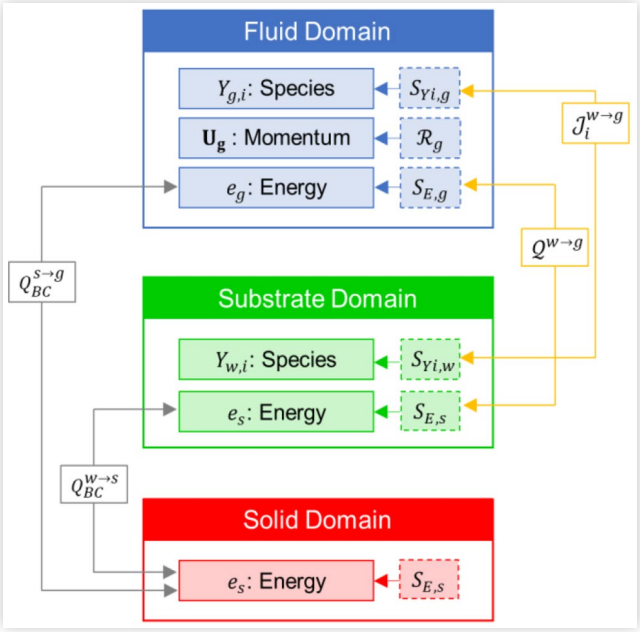

species, with proper source terms: $\mathcal{R}_g$ which includes on the momentum equation the flow resistance induced by the presence of a porous substrate; $S_{Yi,g}$ describing the reaction rates associated to homogeneous reaction occurring in gas phase; $S_{E,g}$ which models the effect the reaction heat released / absorbed by exothermic / endothermic chemical reactions in gas phase. Considering both substrate and solid domains, the energy conservation equation is solved to determine the temperature of the regions and proper source terms $S_{E,s}$ are considered to describe eventual external heating (for example to consider electrical heating). Finally, in the substrate domain, the balance equation for the chemical species on the washcoat surface is solved, considering the internal source term $S_{Yi,w}$ accounting for the reaction rates associated to the catalytic surface reactions.

Moreover, according to this multi-domain framework, specific coupling models should be included to describe the physical interaction between the regions. These can be based on boundary conditions if the coupling is between adjacent regions (fluid to solid, substrate to solid) or on source terms if the coupling is between overlapping regions (fluid to substrate). In particular, boundary conditions are used for the description of wall heat transfer occurring at the interface between the domains. Source terms are applied to describe the inter-phase heat transfer ($\mathcal{Q}^{w\to g}$) and mass transfer ($\mathcal{J}_i^{w\to g}$) occurring in porous substrates between the fluid and the washcoat.

Models for Coupling between Regions

The thermal coupling between adjacent domains is performed by means of a conjugate heat-transfer boundary conditions applied at the fluid-solid or substrate-solid boundary interface. The boundary condition imposes the temperature T_w on the boundary patch of each region i, taking into account temperature and conductivity of the other region j, according to the following relations:

$$T_w = T_i - \frac{\lambda_j L_i}{\lambda_i L_i + \lambda_j L_j}\left(T_i - T_j\right),$$
$$T_w = T_j + \frac{\lambda_i L_j}{\lambda_i L_i + \lambda_j L_j}\left(T_i - T_j\right), \tag{1}$$

where, for fluid and solid regions respectively, L_i and L_j are the distances between cell center and face center at the boundary patch, T_i and T_j are the temperatures in the cell centers and λ_i and λ_j are the conductivities. For fluid domains the conjugate heat-transfer boundary condition can be further coupled with a radiation model as will be described in a next section.

The coupling between overlapping domains is realized by means of source terms. This approach is applied to the modeling of the interaction between fluid and substrate, resorting to correlations available in the literature for the description of the permeability, heat- and mass-transfer of common honeycomb monoliths. In particular, the flow resistance source term $\mathcal{R}_g$ was modeled as:

$$\mathcal{R}_g = f\left(\mathrm{Re}\right)\frac{4}{d_c}\frac{1}{2}\rho U_g^2, \tag{2}$$

where the friction factor is computed according to the Churchill correlation [13]. Similarly, the source terms of heat transfer $\mathcal{Q}^{w\to g}$ and mass transfer $\mathcal{J}_i^{w\to g}$ were computed as:

$$\mathcal{Q}^{w\to g} = \mathrm{Nu}\left(\mathrm{Re},\mathrm{Pr}\right)\frac{\lambda}{d_c}S_V\,V\left(T_g - T_w\right),$$
$$\mathcal{J}_i^{w\to g} = \mathrm{Sh}\left(\mathrm{Re},\mathrm{Sc}\right)\frac{\mathfrak{D}}{d_c}S_V\,V\left(C_g - C_w\right), \tag{3}$$

where Hawthorn correlation has been introduced in order to estimate Nusselt and Sherwood numbers as a function of Reynolds, Prantdl and Schmidt [14, 15].

Model for Surface Catalytic Reactions

The surface reaction model describes the specie conversion occurring on the catalytic washcoat. In order to account for the competition of the chemical species on the active sites, the Langmuir-Hinshelwood type reaction model has been adopted [16]. For the generic reaction i:

$$\alpha A + \beta B \to \gamma C + \delta D, \tag{4}$$

the reaction rate can be expressed as follow:

$$r_i = k_{r,i}\frac{\hat{p}_A\,\hat{p}_B}{T\,G_i}Eq_{f,i} \tag{5}$$

where: $k_{r,i}$ is the Arrhenius term, $\hat{p}_A$ and $\hat{p}_B$ are the partial pressure of reactants divided by the reference pressure, T is the substrate temperature, G_i is an inhibition terms which takes into account the species competition to occupy the active sites and $Eq_{f,i}$ the equilibrium term. The Arrhenius term

describes the dependency of the reaction rate on the temperature and it is calculated as:

$$k_{r,i} = A_{r,i}\, e^{-\frac{E_{r,i}}{RT_w}}. \tag{6}$$

The most of the reactions taking place in catalytic devices are usually non-reversible, therefore the equilibrium term Eq_f is equal to 1. However, some reactions can exhibit a reversible behavior: in order to account for the chemical equilibrium a specific term can be introduced for the forward reaction:

$$Eq_f = 1 - \frac{C_{s,C}^{\gamma}\, C_{s,D}^{\delta}}{C_{s,A}^{\alpha}\, C_{s,B}^{\beta} K_p(T)}. \tag{7}$$

Oxygen Storage Model Cerium plays an important role in TWC since it acts as oxygen storage component through its transition between two different states of oxidation, namely CeO_2 and Ce_2O_3. In particular, during the typical operation of the TWC, which is fed with a mixture which is periodically switching between lean and rich conditions, it stores the oxygen during lean phase and it contributes to the oxidation of carbon monoxide and unburnt hydrocarbon when the mixture is rich [17]. The reaction rates for oxygen storage and release are modeled as:

$$\begin{aligned} R_{storage} &= k\, \hat{p}_i\, \psi_{Ce_2O_3}\, \Psi_{Ce} \\ R_{release} &= k\, \hat{p}_i \left(1 - \psi_{Ce_2O_3}\right) \Psi_{Ce} \end{aligned}, \tag{8}$$

where: k is the Arrhenius term, $\hat{p}_i$ is the partial pressure of reactant, Ψ_{Ce} the total cerium capacity. The term $\psi_{Ce_2O_3}$represents the oxidation state of Ce, ranging between $\psi_{Ce_2O_3} = 0$ (fully oxidized, not possible to store more oxygen) and $\psi_{Ce_2O_3} = 1$ (not oxidized: maximum capability to store oxygen). The evolution of the oxidation state is given by the balance between the activity of the storage and release reactions:

$$\Psi_{Ce} \frac{d\psi_{Ce_2O_3}}{dt} = \sum R_{storage} - \sum R_{release}. \tag{9}$$

The local value of $\psi_{Ce_2O_3}$ is then exploited to determine the actual reaction rate of the catalytic reactions which involve the cerium components CeO_2 and Ce_2O_3.

Radiative Heat Transfer Model The radiation model is included to take into account the radiative heat transfer occurring at high temperatures (> 1000 - 1200 K) between solid components (pipes, canning, substrates, thermocouples, etc) through the fluid domain. The Discrete Ordinates Model (DOM) is adopted to solve the radiative heat transfer problem for a finite number of discrete solid angles in the space. The DOM equations are discretized according to the finite volume method (FVM) exploiting the standard computational grid adopted for the solution of the fluid-dynamic problem. The fluid domain is assumed as a participating media, which can be characterized in terms of absorptivity and emissivity. Solid domains are modeled as opaque, taking into account only their emissivity at the walls.

Solution Algorithm The computational model defined in Figure 2 requires the adoption of a proper solution procedure in order to address the simulation of a typical exhaust line within an acceptable timeframe. As a matter of the fact, the computational size of the problem is significant, due to different factors: a) the size of the problem (i.e. the number of computational cells) which can become significant for typical industrial cases; b) the physical time interval to be simulated, which typically is in the order of minutes - hours (e.g. for the simulation of a cold start condition of a driving cycle) and c) the complexity of the physics to take into account, which requires detailed models as previously described.

For these reasons, the original solution procedure proposed in [7] was further improved, leading to the algorithm reported in Figure 3. In particular, a quasi steady-state approach is implemented, advancing the solution in time according to the characteristic timestep required for an accurate description of the thermal balance of the solid components, being metal walls or substrates. This timestep,

FIGURE 3 Numerical procedure for the solution of the governing equations.

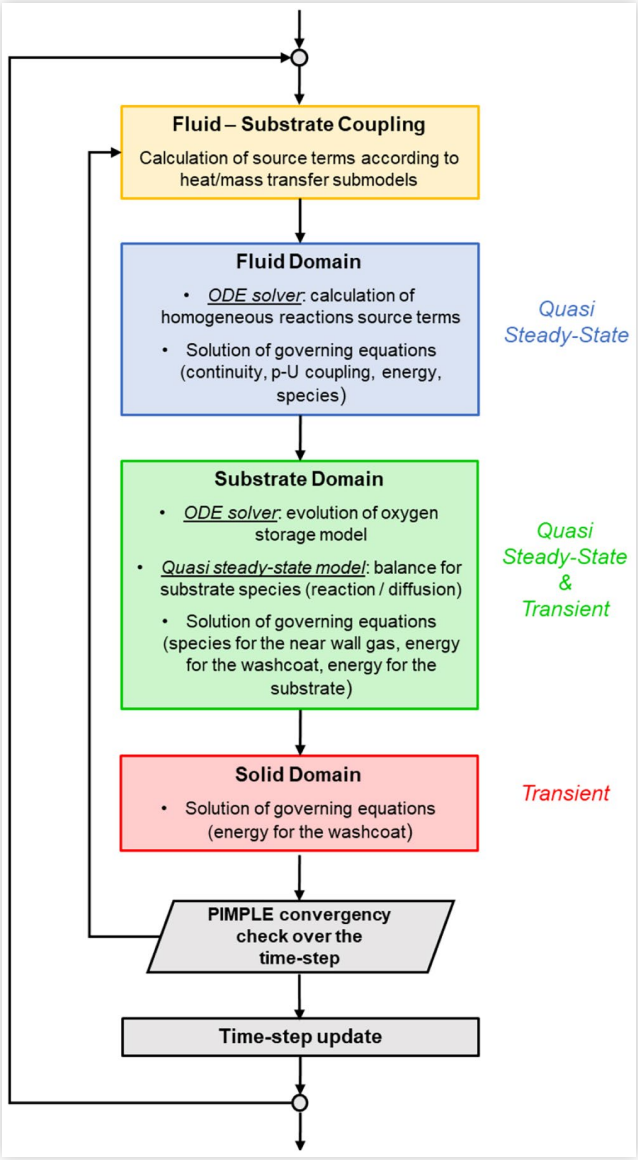

in the range 0.1-1 s, is larger with respect to the characteristic time associated to the fluid-dynamics and chemical reactions and, therefore, cannot be adopted, in principle, for advancing the solution of the governing equations for these phenomena. However, the high frequency content (typical period $10^{-2} - 10^{-3}$ s) associated to the unsteady operation of the engine, related to the unsteady pressure wave propagation, is not usually relevant for the description of the transient behavior of the after-treatment system. Therefore, the boundary conditions for the flow can be properly filtered over a timestep similar to what is required by the thermal analysis. This leads to the modeling of the flow condition in the fluid domain as steady-state over this timestep, allowing the adoption of standard SIMPLE algorithm for its solution.

A similar approach is also applied for the modeling of the surface chemical reactions, assuming the process as quasi steady-state. This hypothesis can be regarded as valid for most of the typical engine operating conditions and implies that the accumulation of reactant / products in the washcoat is negligible. This leads to assume that the rate of diffusion of species to the active catalytic site $\dot{n}_j$ is exactly the same as the rate of the chemical reaction which converts the reactants into product r_j:

$$\dot{n}_j\left(Y_{g,j}, Y_{w,j}, T_g\right) = r_j\left(Y_{w,j}, T_w\right) \tag{10}$$

The above equation is solved iteratively and allows to determine, for each computational timestep, the species concentration on the washcoat surface $Y_{w,j}$ as the result of a stationary balance between diffusion process and chemical reactions. At convergency, the procedure provides, for each species, the concentration at the catalytic sites for which the reaction rate become equal to the diffusion rate under the instantaneous conditions of gas / substrate temperature and gas species concentrations.

A different numerical approach should be adopted for the modeling of the species storage on the washcoat, as in the typical case of oxygen storage in TWC. In this case, the process of storage is intrinsically unsteady with a characteristic period for the cycle of absorption / release of the species in the order of seconds. On the other hand the numerical timestep for an accurate resolution of the process is in the range of $10^{-6} - 10^{-4}$ s. For this reason, an ODE solver should be applied, operating with timestep sub-cycling on the basis of the characteristic time for the chemical phenomena. The same approach is also adopted for the modeling of the homogeneous reactions taking place in the gas phase (i.e. in the fluid domain).

The solution algorithm is structured as follows. For each simulation time-step an iterative procedure is run to obtain the convergency of the solution coupling the different domains. For each iteration, the first operation consists of the coupling between the different overlapping regions, namely fluid and catalyst(s), in order to evaluate substrate permeability and heat- and mass-transfer coefficients. Once the coupling source terms are computed, the equations for the different domains are solved sequentially. When all the operations for the considered iteration are completed, the convergency of the solution over the time-step is checked and, if convergency condition is verified, the time-step is advanced.

Experimental Setup

The experimental data for the validation of the computational model were acquired on a test bench specifically designed for the characterization of the thermal transient of the system when the burner is activated. The after-treatment line was instrumented with a set of K-type thermocouples with external 1.5 mm shield to measure the temperature of the flow. Moreover, thermocouples to measure the temperature of the metal walls were installed. As shown in Figure 4, the thermocouples were located along the flow path from the burner to the catalyst inlet, in order to characterize the cooling of the flow due to thermal inertia of the duct wall and to the external heat-transfer.

Case Study

In this study the after-treatment system for a high-performance V12 engine is considered, dedicated for research purposes. The analysis is focused on one single bank and considers the first section of the system including the primary exhaust ducts and the main catalyst. The exhaust line is equipped with a burner-like system (hereafter referred for sake of simplicity as burner) which is connected through a dedicated pipe to the inlet cone of the catalyst, in such a way to discharge the hot gas in a section located downstream the exhaust manifold. The analysis of the configuration was performed in two steps: at first, a stand-alone simplified exhaust line (Figure 5.a), specifically designed for thermal assessment and validation, was considered and then the analysis was extended to the full configuration (Figure 5.b), in order to evaluate the potential abatement performance of the complex system during engine cold start.

Case A: Simplified Exhaust Line

The reference configuration for the validation consisted in a simplified exhaust line, without manifolds and catalyst. This

FIGURE 4 Schematic showing the experimental setup and the thermocouples positions for the measurement of the gas temperature (blue) and of the metal walls (magenta).

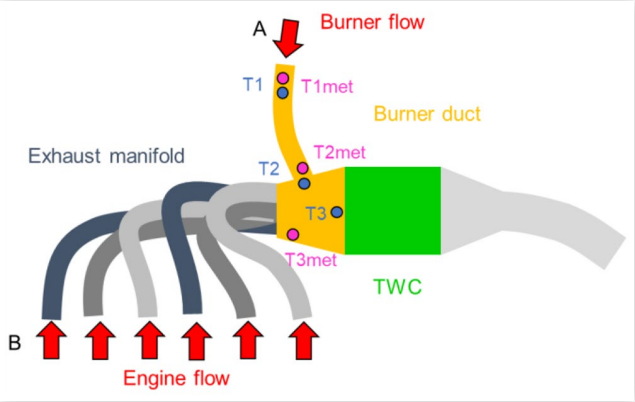

FIGURE 5 Exhaust line configurations: a) stand-alone experimental test bench; b) full exhaust line equipped with manifold and catalyst

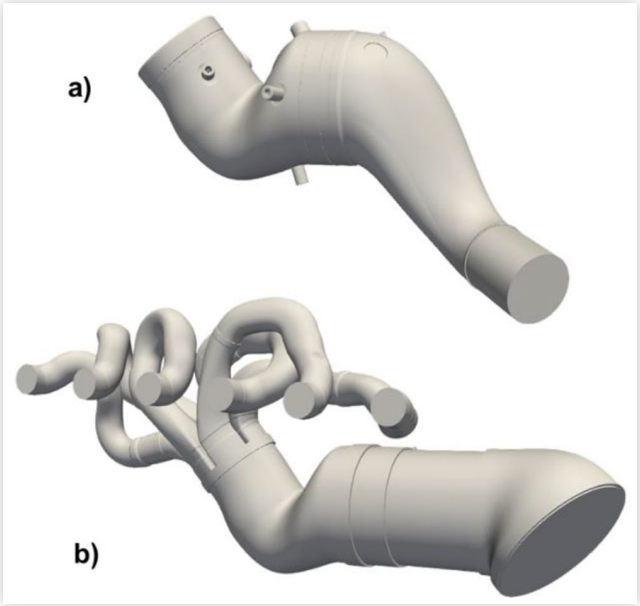

test bench was designed with the aim to provide an accurate characterization of the flow coming from the burner and directed towards the catalyst inlet section. In particular, the investigation is focused on the characterization of the flow field, in terms of velocity and temperature distribution, and on the analysis of the thermal transient of the metallic walls at different locations.

The CFD model was setup according to the multi-region framework including three different domains: one fluid region describing the exhaust gas flow and two solid regions representing respectively the metallic walls of the pipes and the thermocouples. The accurate modeling of the thermocouples geometry was required in order to directly compare with the temperature measured by the real thermocouples installed on the test bench. As a matter of fact, the detailed description of the thermocouples in terms of geometrical and thermal properties allowed to correctly capture the effects related to the thermal inertia of the probe and the heat transfer phenomena (convective / radiative with the surrounding flow field and conductive along the thermocouple). Moreover, the detailed reconstruction of the thickness of the metallic walls of the exhaust line allowed to take into account their thermal inertia, which has a primary role in the dynamics of the thermal transient at the cold start. The details of the multi-region computational mesh are shown in Figure 6. It has been generated adopting snappyHexMesh, an automatic mesh generator included in OpenFOAM which provides a body fitted grid, predominantly consisting of hexahedral cells, with a small percentage of polyhedral elements near the boundary walls. Hexahedral / prism boundary layers have been added to accurately describe near wall flow and thermal gradients. The overall mesh grid consists of $7.8 \cdot 10^6$ cells, grouped as follows: $5.0 \cdot 10^6$ cells for the fluid region, $2.8 \cdot 10^6$ for the metallic walls and $5.4 \cdot 10^4$ for the thermocouples.

FIGURE 6 Detail of the multi-region mesh including thermocouple discretization: fluid domain (blue), metal walls solid domain (red), thermocouple solid domain (gray).

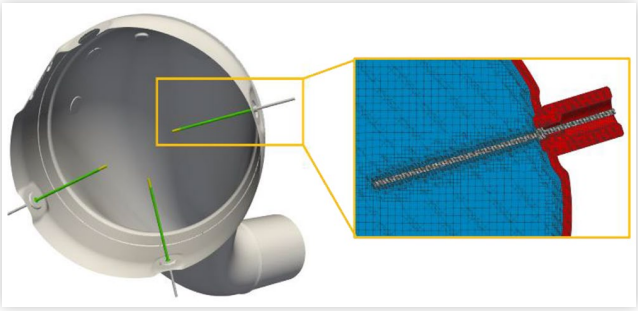

The mesh discretization at the fluid walls was able to guarantee a y^+less than one for all the boundary patches, allowing to employ a low Reynolds turbulence model: hence, the standard k-ω SST turbulence model [18] was applied.

Boundary and initial conditions were imposed on the basis of the experimental measurements performed on the test bench. In particular, at the inlet of the pipe connecting the burner to the catalyst cone (Figure 4, section A) time-varying experimental conditions of mass flow, temperature and chemical composition were imposed. Moreover, convective heat transfer coefficient between metallic walls and external environment was specified according to experimental estimation. Despite the chemical composition was prescribed at the inlet and the transport of the chemical species was solved by the model, chemical reactions were not taken into account at this stage since the catalyst was not included in the experimental configuration. Moreover, also homogeneous gas phase reactions were not included in the model, since their rate is negligible at the typical temperature of the exhaust gas.

Case B: Full Exhaust Line

The second configuration considered in the analysis consisted of a full exhaust line equipped with manifold, burner connecting duct and catalytic substrate. The aim of the investigation was to simulate the operation of the after-treatment system at cold start, evaluating at first the heating phase promoted by the activation of the burner and then the subsequent start of the engine.

The computational grid (Figure 7) was generated according to the multi-region framework, including the overlapped substrate region needed for the modeling of the catalyst. The resulting mesh counts $6.6 \cdot 10^6$ cells for the fluid region, $3.1 \cdot 10^6$ for the metal walls and $2.4 \cdot 10^5$ for the substrate.

The three-way catalyst consisted of a honeycomb ceramic substrate with 800 cpsi and wall thickness equal to 76 µm. Catalytic reactions occurring in the three-way catalyst were described according to the model reported in Table 1, which represents a reasonable starting point when experimental data for the model calibration are not available, as reported in [19].

The simulation was run considering a cold start condition in which at first the burner is activated for 20 s and then the engine is started. Flow boundary conditions were imposed at the inlet of the burner duct (Figure 4, section A) and of the

FIGURE 7 Detail of the multi-region mesh including substrate discretization: fluid domain (blue), metal walls solid domain (red), overlapped substrate domain (green).

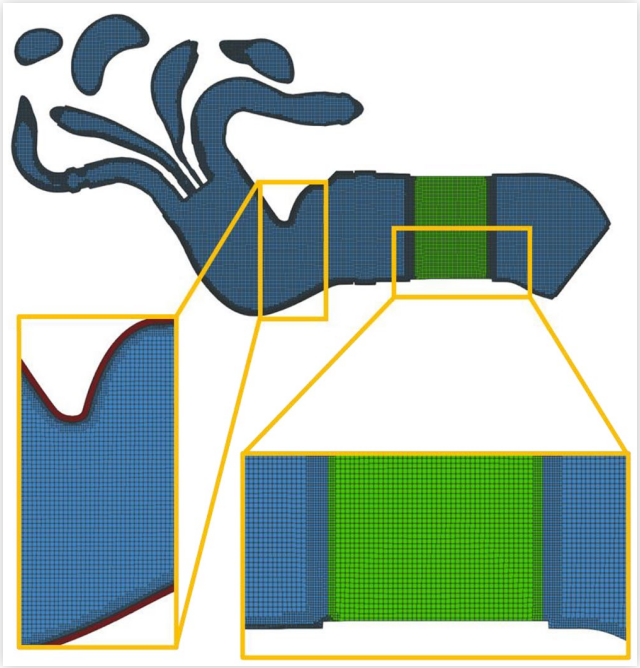

manifold (Figure 4, section B), prescribing instantaneous mass flow, temperature and concentration of the chemical species. All the other parameters were maintained the same as described in the previous section.

Results and Discussion

At first, the numerical model was applied for the simulation of the simplified exhaust line configuration installed on the experimental test bench, with the aim to validate the predictions in terms of fluid-dynamics and heat transfer. Then, the full exhaust line was considered and simulations were run in order to characterize the conversion efficiency of the system in a cold start condition in which the burner is activated before the start of the engine.

Fluid-Dynamics and Thermal Analysis

The validation of the model was conducted considering the simplified configuration installed on the experimental test bench (case A). The instantaneous temperature of the flow at the inlet of the connection duct, which is located immediately downstream the burner, was available from experimental measurements and was imposed as boundary condition for the model (Figure 8, temperature T0). The temperature T0 shows a rapid transient towards the regime value, which is reached after 5 s. In a similar way the mass flow from the burner was imposed in the model as constant during the activation time. The fluid temperature measured experimentally was compared with the temperature estimated by the model on the basis of the detailed reconstruction of the thermocouples. This allowed to directly estimate the temperature of the metal sheath in correspondence of the joint of the thermocouple, enabling the possibility to directly compare with the temperature value provided by the real probe. As a matter of the fact, the "virtual" thermocouple takes into account the thermal inertia and the conductivity of the probe, while the conjugate heat transfer model accurately describes the convective and radiative heat flux exchanged with the fluid domain.

The comparison between calculated and measured temperature can be regarded as satisfactory (Figure 8), both in terms of description of the thermal transient and prediction of the regime temperature. The three probes are located along the flow path between the inlet and the catalyst section (as detailed in Figure 4) and describe the progressive cooling

TABLE 1 Reaction scheme for the modeling of the TWC.

		Ar,i	*Er,i*
R1	$CO + \frac{1}{2}O_2 \rightarrow CO_2$	$1.00 \cdot 10^{20}$	$1.00 \cdot 10^{5}$
R2	$H_2 + \frac{1}{2}O_2 \rightarrow H_2O$	$5.00 \cdot 10^{20}$	$1.00 \cdot 10^{5}$
R3	$C_3H_6 + \frac{9}{2}O_2 \rightarrow 3CO_2 + H_2O$	$5.00 \cdot 10^{19}$	$9.00 \cdot 10^{4}$
R4	$C_3H_8 + 5O_2 \rightarrow 3CO_2 + 4H_2O$	$1.00 \cdot 10^{16}$	$1.20 \cdot 10^{5}$
R5	$C_3H_6 + 9NO \rightarrow 3CO_2 + 3H_2O + \frac{9}{2}N_2$	$1.00 \cdot 10^{14}$	$9.00 \cdot 10^{4}$
R6	$CO + NO \rightarrow CO_2 + \frac{1}{2}N_2$	$5.00 \cdot 10^{14}$	$7.00 \cdot 10^{4}$
R7	$H_2 + NO \rightarrow H_2O + \frac{1}{2}N_2$	$5.00 \cdot 10^{15}$	$7.00 \cdot 10^{4}$
R8	$CO + H_2O \rightarrow CO_2 + H_2$	$1.00 \cdot 10^{9}$	$7.00 \cdot 10^{4}$
R9	$CO_2 + H_2 \rightarrow CO + H_2O$	$1.00 \cdot 10^{9}$	$7.00 \cdot 10^{4}$
R10	$C_3H_6 + 3H_2O \rightarrow 3CO + 6H_2$	$9.00 \cdot 10^{11}$	$8.00 \cdot 10^{4}$
R11	$C_3H_8 + 3H_2O \rightarrow 3CO + 7H_2$	$9.00 \cdot 10^{12}$	$1.00 \cdot 10^{5}$
R12	$Ce_2O_3 + \frac{1}{2}O_2 \rightarrow 2CeO_2$	$5.00 \cdot 10^{11}$	$1.50 \cdot 10^{5}$
R13	$Ce_2O_3 + NO \rightarrow 2CeO_2 + \frac{1}{2}N_2$	$3.00 \cdot 10^{13}$	$1.60 \cdot 10^{5}$
R14	$2CeO_2 + CO \rightarrow Ce_2O_3 + CO_2$	$5.00 \cdot 10^{8}$	$1.20 \cdot 10^{5}$
R15	$2CeO_2 + H_2 \rightarrow Ce_2O_3 + H_2O$	$5.00 \cdot 10^{8}$	$1.20 \cdot 10^{5}$
R16	$2CeO_2 + \frac{1}{6}C_3H_6 \rightarrow Ce_2O_3 + \frac{1}{2}CO + \frac{1}{2}H_2O$	$1.00 \cdot 10^{12}$	$1.50 \cdot 10^{5}$
R17	$fCe_2O_3 + \frac{1}{2}O_2 \rightarrow 2fCeO_2$	$3.50 \cdot 10^{10}$	$1.00 \cdot 10^{5}$
R18	$fCe_2O_3 + NO \rightarrow 2fCeO_2 + \frac{1}{2}N_2$	$5.00 \cdot 10^{12}$	$1.00 \cdot 10^{5}$
R19	$2fCeO_2 + CO \rightarrow fCe_2O_3 + CO_2$	$5.00 \cdot 10^{8}$	$8.00 \cdot 10^{4}$
R20	$2fCeO_2 + H_2 \rightarrow fCe_2O_3 + H_2O$	$5.00 \cdot 10^{8}$	$8.00 \cdot 10^{4}$
R21	$2fCeO_2 + \frac{1}{6}C_3H_6 \rightarrow fCe_2O_3 + \frac{1}{2}CO + \frac{1}{2}H_2O$	$5.00 \cdot 10^{8}$	$8.00 \cdot 10^{4}$
R22	$2fCeO_2 + \frac{1}{7}C_3H_8 \rightarrow fCe_2O_3 + \frac{3}{7}CO + \frac{4}{7}H_2O$	$2.00 \cdot 10^{6}$	$8.00 \cdot 10^{4}$

FIGURE 8 Temperature of the exhaust gas at different locations, as specified in Figure 4: validation of the calculated data against experimental measurements. Data are non-dimensionalized with respect to minimum and maximum temperature.

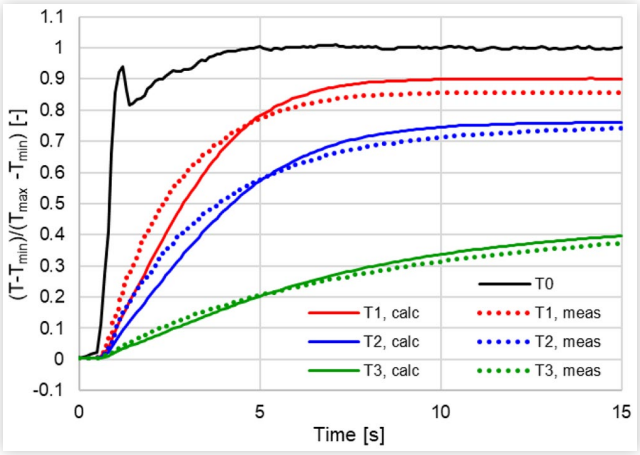

of the burner exhaust gases before reaching the catalyst. This is mainly due to the convective heat transfer between the gas flow and the pipe walls, which are progressively heated increasing their temperature starting from the initial cold condition. The thermal heating of the metallic walls is characterized in Figure 9, where experimental and calculated solid temperatures are compared at three different locations. Also in this case thermocouples are distributed between the burner connection and the catalyst location, in such a way to describe the temperature non-uniformity of the metallic walls (Figure 4). The comparison shows a good agreement between measurements and calculations. It can be noticed that the temperature of the metal walls is increasing progressively due to the heat transferred from the fluid; however, the final value reached in the considered time interval (15 s) is significantly lower than the fluid temperature and is far from the regime condition.

FIGURE 9 Temperature of the metal walls at different locations: validation of the calculated data against experimental measurements. Data non-dimensionalization consistent with Figure 8.

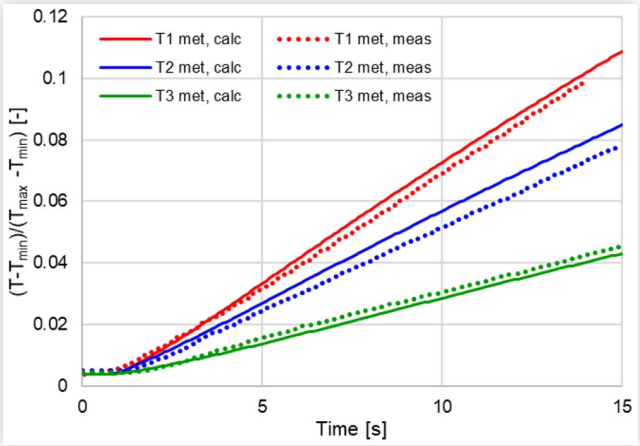

FIGURE 10 Comparison of the temperature of the exhaust gas calculated with and without radiation model. Data non-dimensionalization is the same as Figure 8.

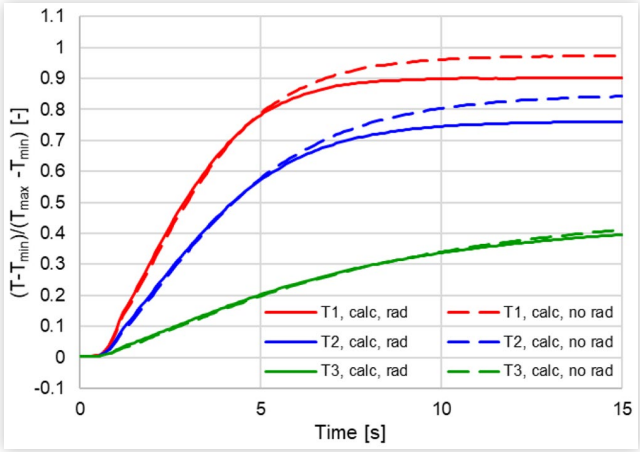

This is mainly due to the thermal inertia of the metallic walls which, in this phase, is largely predominant over the external convective heat transfer towards the environment.

As further analysis, the role of the radiative heat transfer is evaluated. Figure 10 reports the comparison of the numerical estimation of the thermocouple temperatures when the radiative heat transfer model is disabled. It can be noticed that the larger differences are found at the highest temperatures, where the contribution of the radiative heat transfer is significant. In particular, for the first probe location (T1) it can be seen that the radiative heat transfer is the main responsible for the reduction of the probed temperature at regime condition with respect to the inlet value. On the other hand, at lower temperature (as for probe T3) the effect of radiative heat transfer becomes negligible.

In Figure 11 the temperature distribution in the section where the catalyst should be placed (A) and in two other

FIGURE 11 Flow temperature distribution downstream the inlet cone for the catalyst (not included in the test bench configuration) for time 10 s.

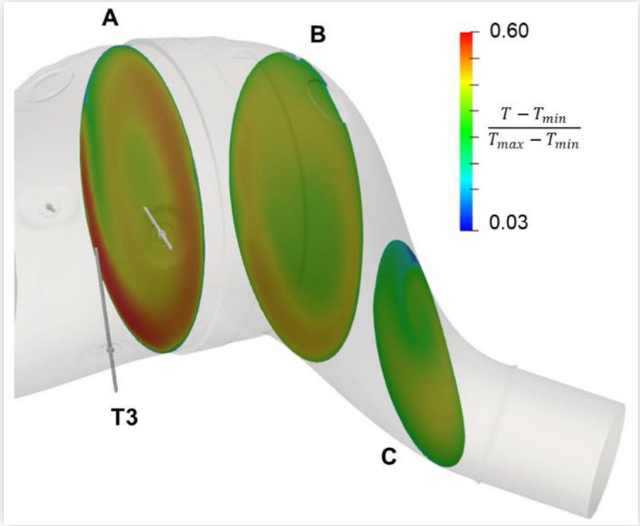

sections downstream (B, C) is reported. The section A is close to the position of the thermocouple T3 discussed with reference to the previous graphs. The temperature field shows a certain degree of non-uniformity, related to the fact that the configuration adopted here for the validation of the model was not specifically designed to optimize this aspect. However, from the validation point of view, this test condition is significant because it shows the capability of the model of predicting the non-uniform flow distribution, as assessed by the combination of the information coming from thermocouple T3 (which experiences the lower temperature) and the wall thermocouple T3met (which measures the temperature of the wall in contact with the flow stream characterized by the highest temperatures).

Full Cold-Start Analysis

After the first validation step, the CFD model was applied for the investigation of a full cold start transient with burner activation conditions and subsequent start of the engine. Even though the experimental data were not available for this specific tested condition, the numerical analysis was performed on the basis of the data available from the experimental characterization of the burner out (as described in the previous section) and of the engine out (as measured in configurations without burner). Time-dependent boundary conditions were applied at the inlet of the burner duct and of the exhaust manifold. Figure 12 reports mass flow and gas temperature boundary conditions imposed at the burner out and engine out, while raw emissions can be found in Figures 16-18. The tested condition considers a first heating step, in which the burner is activated for 20 s, and a subsequent phase in which burner is deactivated and the engine is started. Simulation is run for total 50 s.

Figure 13 shows the temperature and velocity fields on a transversal section of the system 10 s after the engine start. It can be seen that the flow coming from the exhaust manifold is cooled due to the heat exchanged with the pipe walls, while

FIGURE 12 Boundary conditions applied at the inlet of the burner duct and of the exhaust manifold for mass flow and gas temperature. The engine starts at 20 s and the burner is completely switch-off at 22.5 s.

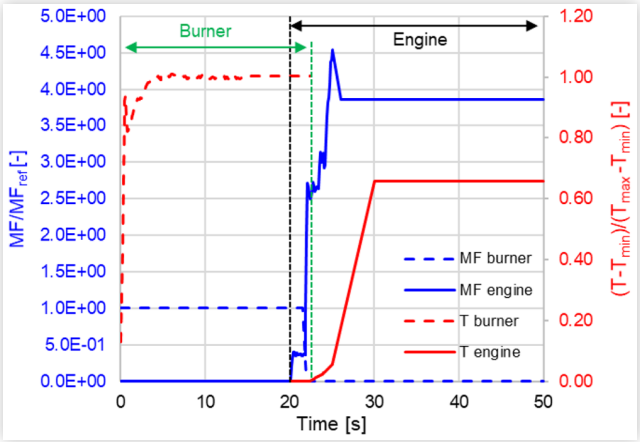

FIGURE 13 Temperature and flow condition at 30 s (10 s after the engine start) for a transversal section of the ATS including the TWC (highlighted with black line).

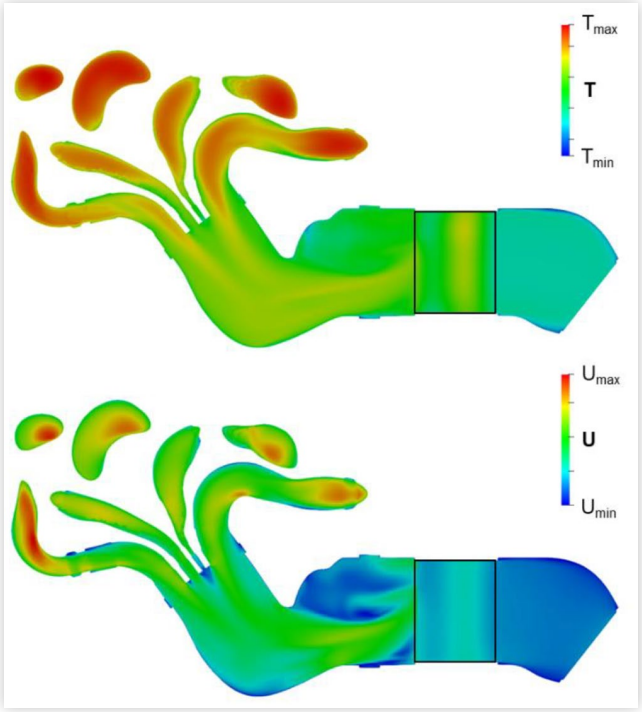

a high temperature region can be noticed in the second half of the catalyst. This high temperature zone is the result of the previous heating of the substrate due to the burner activation. On the other hand, the lower temperature in the first section of the substrate is due to the cooling associated to the cold flow coming from the engine during the cranking phase. The temperature distribution inside the substrate determines also the non-uniform flow velocity along the catalyst axis, which is related to the different gas density.

The tracking of the pollutant chemical species for the same time (10 s after the engine start) is reported in Figure 14. At this time, the temperature of the substrate is already sufficient to enable the light-off of all the catalytic reactions, determining the abatement of the pollutants in the first part of the TWC. Moreover, the low engine mass flow during the start condition contributes to the efficiency of the overall abatement, which is slightly more effective for CO and HC with respect to NO_x.

The temperature of the substrate during the cold start transient is monitored in Figure 15, where four different locations are considered along the catalyst axis. During the activation of the burner (time < 20 s) the temperature of the substrate is rising with different rates for the different locations: the heating is quite fast for the first section at the catalyst inlet, while it is negligible in the second part of the catalyst. The thermal inertia of the substrate plays a key role, influencing the extension of the zone where the temperature reaches a sufficient value for the light-off of the reactions. In this phase, the conversion of the pollutant emissions from the burner is not a crucial point, as can be seen in Figures 16, 17, 18: as a matter of fact, the CO and HC emissions are negligible, since

FIGURE 14 Pollutants mass fractions at 30 s (10 s after the engine start) for a transversal section of the ATS including the TWC (highlighted with black line).

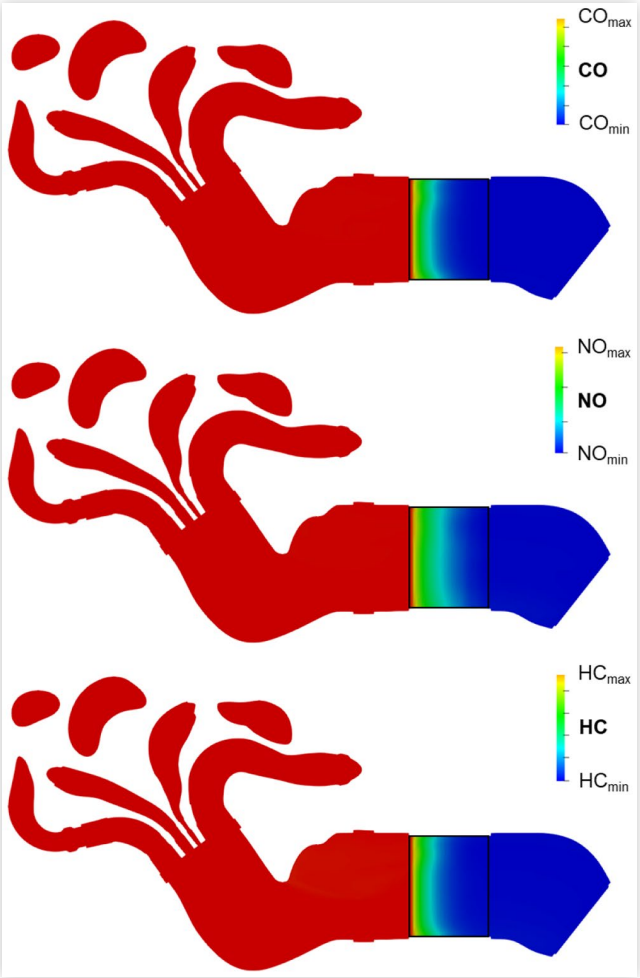

FIGURE 15 Solid temperature evolution in different locations along the axis of the substrate: inlet section of the TWC, 25 mm downstream the inlet section, mid section, outlet section. Data non-dimensionalization is consistent with Figure 12.

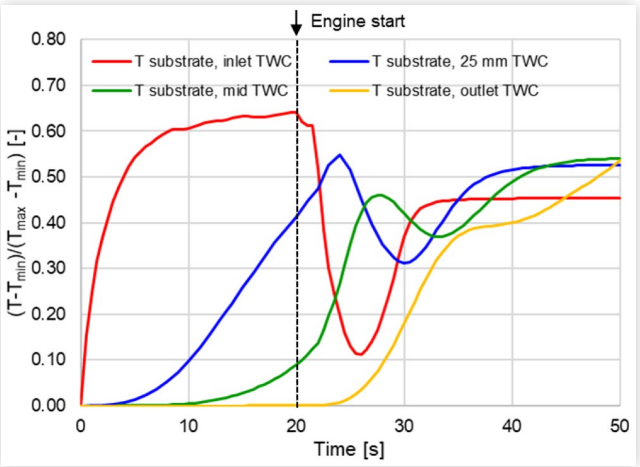

FIGURE 16 Evolution of the CO emission during the engine cold start with burner activation: cumulative emission (dashed blue line: inlet, continuous blue line: outlet) and conversion efficiency (red line).

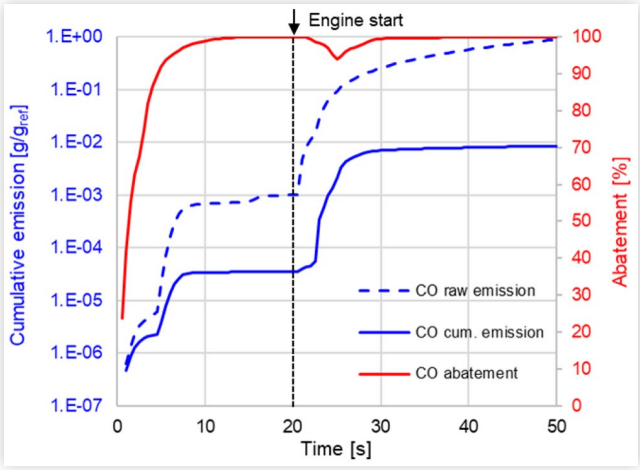

FIGURE 17 Evolution of the NOx emission during the engine cold start with burner activation: cumulative emission (dashed blue line: inlet, continuous blue line: outlet) and conversion efficiency (red line).

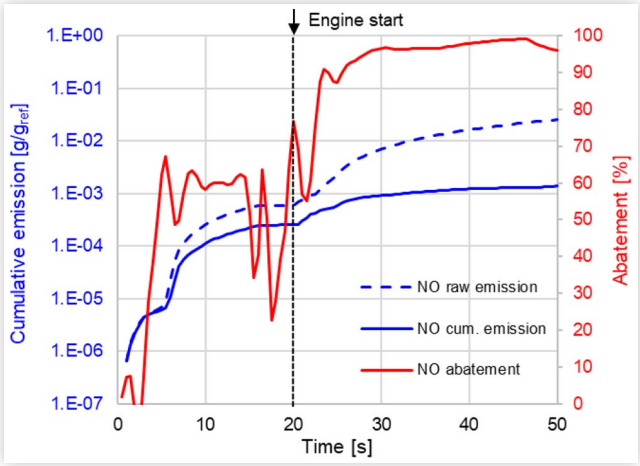

the burner is operated in lean condition, while the NO_x emission can be controlled quite effectively even if the reactions are active only in a restricted portion of the catalyst. After 20 s, when the burner is turned off and the engine is started, the substrate temperature shows a reduction due to the cooling effect of the exhaust gas flow from the engine, which has a low temperature during the cranking phase. The cooling takes place with a certain time delay passing from the inlet location and moving forward to the downstream probe locations. Then, in the next few seconds, the exhaust gas temperature starts to increase, even if slowly due to the cooling effects of the cold metallic walls. However, the increase of the exhaust gas temperature is enough to determine the heating of the substrate temperature in the first section which was subjected to the strongest cooling. Moreover, exothermic catalytic reactions start to take place in the zone where the

FIGURE 18 Evolution of the HC emission during the engine cold start with burner activation: cumulative emission (dashed blue line: inlet, continuous blue line: outlet) and conversion efficiency (red line).

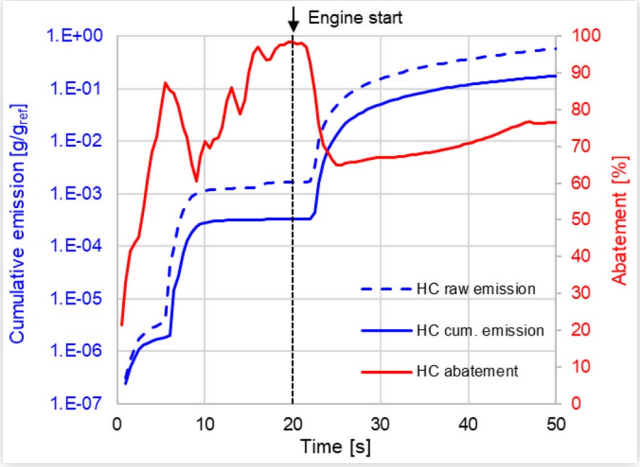

temperature is higher, contributing to a further increase of the substrate temperature. This effect is evident after 35 s, when the temperature of the substrate in the central part and second half portion of the TWC reaches a higher temperature with respect of the inlet section.

Cumulative emissions show a trend which is consistent with the substrate temperature evolution described so far. For all the pollutants, the most critical phase is in the range 20-30 s, when the engine starts and the exhaust gases exhibit a low temperature which has a cooling effect of the substrate. Then, the activity of the catalyst increases in the range 30-50 s, even if different abatement levels are registered for the different pollutants: at 50 s the CO abatement is > 99%, NO is around 97%, HC around 76%. The lower abatement level reached by HC is due to the higher light-off temperature required by the catalytic abatement of this pollutant.

The evolution of the substrate temperature field during the cold start of the engine is reported in Figure 19. Time 21.5 s shows the starting temperature distribution when the burner is deactivated, which exhibits a maximum temperature in correspondence of the inlet section of the catalyst. Then, in time range 22.5 - 27.5 s, the exhaust gas flow coming from the engine, which is characterized by low temperature due to the heat exchange with the cold metallic walls of the manifold, determines a significant cooling of the substrate. In particular, the cooling is more significant for the zone near the inlet section, while the highest temperature region is progressively moved downstream. For time > 30 s, the temperature of the exhaust gas starts to increase while, at the same time, the exothermic reactions with lower activation energy (i.e. CO oxidation) are occurring in the zones characterized by the highest temperature. This results in a progressive light-off of the catalyst starting from the central part of the substrate.

The simulation of the full exhaust line was run in parallel employing 4 to 28 processors, applying domain decomposition on all the three regions, and exhibiting a good scalability. The overall computational runtime for simulating 50 s was around 130 h on 28 processors.

FIGURE 19 Solid temperature evolution in the substrate during the engine cold start.

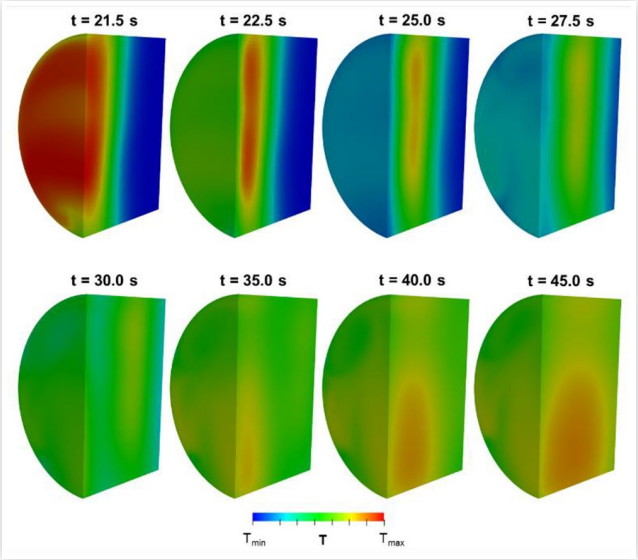

Conclusions

In this paper an after-treatment system including a burner-like system as heating device has been studied applying a numerical modeling approach. The main findings and conclusions of the work are hereafter summarized:

1. A comprehensive CFD numerical model has been implemented for the simulation of the exhaust after-treatment system. The model, based on a multi-region approach for the description of the different domain (fluid, metal walls, substrates, thermocouples) allows the detailed description of the heat-transfer phenomena between the regions (including: conduction, convection and radiation), allowing an accurate prediction of the transient heating of the device at cold start. Moreover, a catalyst model based on quasi steady-state assumption is implemented, allowing to consider arbitrary reaction schemes for the modeling of the surface reactions. The implemented solution algorithm allows to keep the computational burden low, in such a way to make it possible the simulation of relatively long time intervals (in the order of minutes / hours) also exploiting massive parallelization. These aspects make the developed simulation methodology particularly interesting for the design of the next generation ATS in view of the upcoming Euro 7 legislation, as numerical optimization tool to be applied in supporting and guiding the experimental tests.
2. Experimental activity performed on a dedicated test bench was exploited for the validation of the CFD model. Moreover, the combination of experimental data and simulation results allowed to obtain additional information about the pre-heating effects on the after-treatment behavior. The analysis confirms that the thermal inertia of the metal walls

plays a primarily role in the cooling of the gas from the burner during all the pre-heating phase. Furthermore, the model confirms that at high temperature it is important to consider heat transferred by radiation, which has a significant influence on the measured gas temperature.

3. A complete after-treatment line, equipped with a burner-like system and catalyst, was simulated considering a full cold start transient. The tested condition included the burner heating phase and the subsequent start of the engine, describing the light-off of the catalytic reactions. The simulation shows that the burner is a possible solution for the speed-up of the thermal transient, increasing the temperature and so the abatement efficiency of the catalyst before the engine starts. However, the simulation pointed out that the early phase of the engine start can be critical, since the exhaust gas is subjected to a strong cooling due to the interaction with the cold manifold. This determines a cooling of the catalyst, which was previously preheated by the burner. However, a hot region in the mid of the catalyst is preserved, giving a significant spur to the light-off of the reactions when the concentration of the pollutants in the exhaust gas increased.
4. The results shown in this paper, obtained by means of a numerical investigation, should be regarded as a promising starting point for the development and the implementation of such layout on the vehicle, pointing out how a pre-heating device influences the aftertreatment response and efficiency in time. However, it should be remarked that, currently, the burner catalyst technology as a specific component is still confined at a research stage. Further studies and investigations will be addressed to evaluate its actual potential for production cars, also defining the targets for a burner device compliant with the wide range of operating conditions required by the automotive community.

References

1. Sterlepper, S., Claßen, J., Pischinger, S., Görgen, M. et al., "Relevance of Exhaust Aftertreatment System Degradation for EU7 Gasoline Engine Applications," SAE Technical Paper 2020-01-0382 (2020). https://doi.org/10.4271/2020-01-0382.
2. Joshi, A., "Review of Vehicle Engine Efficiency and Emissions," *SAE Int. J. Advances & Curr. Prac. in Mobility* 2, no. 5 (2020): 2479-2507.
3. Yusuf, A.A. and Inambao, F.L., "Effect of Cold Start Emissions from Gasoline-Fueled Engines of Light-Duty Vehicles at Low and High Ambient Temperatures: Recent Trends," *Case Studies in Thermal Engineering* 14: 100417, 2019.
4. Raman, V., Viollet, Y., and Chang, J., "Development of Fast Idle Catalyst Light-Off Strategy for Gasoline Compression Ignition Engine - Part 1," SAE Technical Paper 2020-01-0316 (2020). https://doi.org/10.4271/2020-01-0316.
5. Luo, X., Hashemi, S., Subramanian, R., and Arvanitis, A., "Fast Catalyst Light-Off with Dynamic Skip Fire," *SAE Int. J. Advances & Curr. Prac. in Mobility* 2, no. 4 (2020): 1849-1861.
6. Hofstetter, J., Boucharel, P., Atzler, F., and Wachtmeister, G., "Fuel Consumption and Emission Reduction for Hybrid Electric Vehicles with Electrically Heated Catalyst," *SAE Int. J. Advances & Curr. Prac. in Mobility* 3, no. 1 (2021): 702-714.
7. Della Torre, A., Montenegro, G., Onorati, A., and Cerri, T., "CFD Investigation of the Impact of Electrical Heating on the Light-off of a Diesel Oxidation Catalyst," SAE Technical Paper 2018-01-0961 (2018). https://doi.org/10.4271/2018-01-0961.
8. Hepburn, J., Adamczyk, A., and Pawlowicz, R., "Gasoline Burner for Rapid Catalyst Light-Off," SAE Technical Paper 942072 (1994). https://doi.org/10.4271/942072.
9. Hayashi, S., Akai, M., and Iwai, N., "Study on the Intermittent Dual-Fluid Exhaust Burner (Ideb)-Burner System Without Fuel Supply Device and Air Blower for Rapid Catalyst Heating," SAE Technical Paper 958621 (1995). https://doi.org/10.4271/958621.
10. zu Schweinsberg, A., Klenk, M., and Degen, A., "Engine-Independent Exhaust Gas Aftertreatment Using a Burner Heated Catalyst," SAE Technical Paper 2006-01-3401 (2006). https://doi.org/10.4271/2006-01-3401.
11. Weller, H., Tabor, G., Jasak, H., and Fureby, C., "A Tensorial Approach to CFD using Object Orientated Techniques," *Computers in Physics* 12, no. 6 (1998): 620.
12. Della Torre, A., Montenegro, G., Onorati, A., Cerri, T. et al., "Numerical Optimization of a SCR System Based on the Injection of Pure Gaseous Ammonia for the NOx Reduction in Light-Duty Diesel Engines," SAE Technical Paper 2020-01-0356 (2020). https://doi.org/10.4271/2020-01-0356.
13. Churchill, S.W., "Comprehensive Correlating Equations for Heat, Mass and Momentum Transfer in Fully Developed Flow in Smooth Tubes," *Ind. Eng. Chem. Fundam.* 16 (1977): 109-116.
14. Montenegro e, G. and Onorati, A., "1D Thermo-Fluid Dynamic Modeling of Reacting Flows inside Three-Way Catalytic Converters," *SAE Int. J. Engines* 2, no. 1 (2009): 1444-1459.
15. Wieting, A.R., "Empirical Correlations for Heat Transfer and Flow," *Journal of Heat Transfer* 97 (1975): 488-490.
16. Koltsakis, G., Konstantinidis e, P., and Stamatelos, A., "Development and Application Range of Mathematical Models for 3-Way Catalytic Converters," *Applied Catalysis B: Environmental* 12, no. 2-3 (1997): 161-191.
17. Tsinoglou, D., Koltsakis, G., and Jones, G.P., "Oxygen Storage Modeling in Three-Way Catalytic Converters," *Industrial & Engineering Chemistry Research* 41, no. 5 (2002): 1152-1165.
18. Menter, F.R., "Two-Equation Eddy-Viscosity Turbulence Models for Engineering Applications," *AIAA Journal* 32, no. 8 (1994): 1598-1605.
19. Della Torre, A., Montenegro, G., Onorati, A., Paltrinieri, S. et al., "Calibration of the Oxygen Storage Reactions for the Modeling of an Automotive Three-Way Catalyst," *Industrial & Engineering Chemistry Research* 20, no. 18 (2021): 6653-6661.

Contact Information

Dr. Augusto Della Torre
Department of Energy, Politecnico di Milano
Via Lambruschini, 4
20156 Milano, Italy
phone: +39 02 2399 8631
augusto.dellatorre@polimi.it

Acknowledgments

The authors gratefully acknowledge financial support from "Fondi europei della Regione Emilia-Romagna", within programs POR FESR e POR FSE 2014-2020 in the framework of the "Accordo Regionale di insediamento e sviluppo delle imprese - progetto STEP".

Definitions and Abbreviations

- $\blacksquare_g$ - Gas phase (sub-/super-script)
- $\blacksquare_w$ - Washcoat phase (sub-/super-script)
- $\blacksquare_s$ - Solid phase (sub-/super-script)
- $\blacksquare^{w\to g}$ - Washcoat to gas (super-script)
- $\blacksquare^{w\to s}$ - Washcoat to solid (super-script)
- $\blacksquare^{s\to g}$ - Solid to gas (super-script)
- $\boldsymbol{\rho}$ - Density
- $\mathbf{U}$ - Velocity vector
- $\boldsymbol{e}$ - Internal energy
- $\boldsymbol{T}$ - Temperature
- $\boldsymbol{t}$ - Time
- $\boldsymbol{Y_i}$ - Chemical species mass fraction
- $\boldsymbol{C_i}$ - Chemical species concentration
- $\boldsymbol{\lambda}$ - Thermal conductivity
- $\mathfrak{D}$ - Species diffusivity
- $\boldsymbol{S}$ - Generic source term
- $\mathcal{R}$ - Fluid-dynamic resistance source term
- $\mathcal{Q}$ - Heat source term
- $\mathcal{J}_i$ - Species mass source term
- $\boldsymbol{r_i}$ - Reaction rate
- $\boldsymbol{A_{r,i}}$ - Pre-exponential factor
- $\boldsymbol{E_{r,i}}$ - Activation energy
- $\boldsymbol{G_i}$ - Inhibition term
- $\boldsymbol{d_c}$ - Characteristic dimension of an element
- **Re** - Reynolds number
- **Pr** - Prandtl number
- **Nu** - Nusselt number
- **Sh** - Scherwood number
- **Sc** - Schmidt number
- **TWC** - Three-way catalyst

ISSN 0148-7191